Millimeter-wave Full-Duplex Wireless: Applications, Antenna Interfaces and Systems

(Invited Paper)

Tolga Dinc, Harish Krishnaswamy
Dept. of Electrical Engineering, Columbia University, New York, NY 10027, USA

***Abstract*—Millimeter-waves offer significantly wider channel bandwidths (BW) than RF and are drawing significant interest for short-range wireless personal area networks (WPANs), vehicular radar and next generation (5G) cellular communication. Full-duplex is another emergent technology which can theoretically double the data capacity by transmitting and receiving simultaneously on the same frequency. This paper reviews recent developments at Columbia University on millimeter-wave full-duplex which merges these two emergent technologies. In this context, potential applications for millimeter-wave full-duplex links are described. A 60GHz full-duplex transceiver and 25GHz magnetic-free non-reciprocal passive circulator implemented in 45nm SOI CMOS are discussed. The 60GHz full-duplex transceiver employs polarization-based antenna and RF cancellation to achieve almost 80dB self-interference (SI) suppression. The 25GHz circulator is based on spatio-temporal conductivity modulation and achieves 3.2dB insertion loss, >18.3dB isolation (limited by the measurement setup) over a 4.6GHz 1dB insertion loss (IL) BW, and an input P1dB of >20dBm. Finally, topics for future research are discussed.**

I. Introduction

Millimeter-wave circuits and systems have been traditionally implemented in expensive III-V compound semiconductor technologies. The rapid maturation of silicon technologies has enabled the exploration of silicon-based millimeter-wave circuits and systems for short-range 60GHz WPANs [1], now standardized as WiGig or IEEE 802.11ad. WiGig promises high data rates up to 7Gbps for applications ranging from HD multimedia streaming and gaming to virtual reality. Silicon-based millimeter-wave technology has also been adopted in the design of automotive radars in the recent years [2], [3]. It is likely to become even more prevalent in the future with next-generation (5G) cellular communication on its way.

In the context of next-generation cellular networks (5G), a 1000-fold increase in data traffic is projected over the next 10 years as demand for wireless network capacity keeps doubling every year [4]. Solutions for delivering the 1000-fold increase in capacity fall into three main categories: deploying smaller cells (especially in urban settings), allocating more spectrum and improving spectral efficiency [5]. Smaller cells at low carrier frequencies (1-5GHz) are unlikely to deliver the demanded capacity increase due to interference and spectrum limitations at these frequencies [6]. On the other hand, millimeter-wave frequencies (30-300GHz) allow integration of interference mitigation techniques (e.g. phased arrays) in a smaller form-factor and offer wider, multi-GHz channel bandwidths. Therefore, millimeter-wave beam-forming has recently gained significant research interest as one of the most promising solutions to address the data traffic demands of 5G.

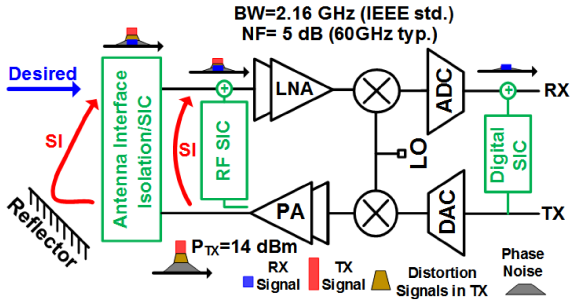

Fig. 1. A typical full-duplex transceiver block diagram. In a 60GHz FD transceiver, a self-interference suppression higher than 96dB is required, assuming transmit power of +14dBm, NF of 5dB and 2.16GHz channel BW.

Another emergent technology in the recent years is same-channel full-duplex, which will be referred to as just full-duplex (FD) in this paper. FD can theoretically double the spectral efficiency over time division duplex (TDD) or frequency division duplex (FDD) in the physical layer through simultaneous transmission and reception on the same frequency channel (Fig. 1).[1] In addition to capacity gain over half-duplex, FD paves the way for revolutionizing wireless protocol design and hence can offer many other new benefits in the higher layers [9]. Although FD promises great benefits for communication systems, self-interference (SI) from the transmitter to its own receiver poses a fundamental challenge. The SI can be more than a billion times stronger than the weak desired signal and must be suppressed below the receiver noise floor to enable full-duplex operation [10]. For example, an FD transceiver at 60GHz with a typical transmit power of +14dBm, receiver noise figure of 5dB and channel BW of 2.16GHz would require +14dBm-(-174 dBm/Hz+10log(2.16GHz)+5)+6=96dB of self-interference cancellation (SIC), assuming a 6dB margin. This suppression must be achieved in antenna, RF/analog and digital domains.

In the rest of this paper, we will first discuss the applications for millimeter-wave full-duplex and then review recent research at Columbia University to enable millimeter-wave full-duplex operation, namely a 60GHz FD transceiver based on polarization-based antenna and RF cancellation [11], [12] as well as a near-28GHz low-loss, wide BW magnetic-free non-reciprocal passive circulator [13] based on spatio-temporal

[1]Interference between cells and asymmetric uplink and downlink traffic are factors that must be considered when evaluating the capacity gain achieved through FD [7]. Research is ongoing to design resource allocation algorithms that maximize capacity gains under these contraints [8].

978-1-5090-5191-5/17/$31.00@2017 IEEE

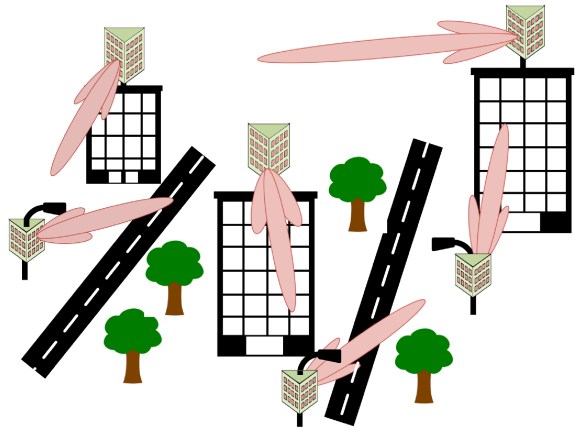

Fig. 2. A 60GHz phased-array-based FD backhaul mesh network can support up and down links simultaneously on the same channel, improving spectral efficiency and reducing latency.

conductivity modulation.

II. Millimeter-wave Full-duplex Applications

A. Millimeter-wave FD Backhaul

Backhaul is one of the least addressed bottlenecks of future 5G wireless communication. Rapid growth of mobile data traffic in 5G wireless communication networks will bring great capacity pressure on the backhaul. Therefore, connecting 5G base stations to other 5G base stations and the network through low-latency, cost-effective backhauling mechanisms with fiber-like throughput is essential [14]. Fiber is the dominant technology for backhaul due to virtually unlimited capacity and link distance but it is hard and costly to deploy. Therefore, bringing fiber to every 5G small cell looks prohibitively expensive [15]. On the other hand, E-band microwave backhaul has been explored in the recent years as a cost-effective method to deliver Gbps throughput. However, it uses two different bands for simultaneous uplink and downlink (effectively FDD between 71-76GHz and 81-86GHz through the use of waveguide diplexers), and high-gain Cassegrain antennas to support extremely long link ranges in adverse weather conditions, resulting in static links and networks that require careful alignment. In the recent past, there has been interest in phased-array-based backhaul in the unlicensed 60GHz band over shorter distances between densely deployed base stations (Fig. 2) [16]. Phased arrays reduce installation costs and enable interference mitigation. Simultaneous uplink and downlink is necessary to reduce latency, and FD operation would enable such operation using a single frequency band.

B. Millimeter-wave Small-cell 5G Base-Stations

Millimeter-wave small-cell 5G base-stations are envisioned to increase coverage in dense areas and will need to communicate with multiple users simultaneously in uplink and downlink. Although the multiple users will occupy adjacent channels in the same band, the techniques developed in the context of FD for front-end transmitter-receiver (TX-RX) isolation will be important. For example, a fully-integrated low-loss, high isolation circulator with high power handling capability would be useful to share a single antenna between

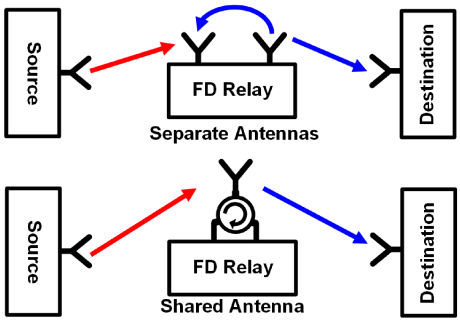

Fig. 3. Millimeter-wave FD relaying with separate TX and RX antennas or shared antenna with a millimeter-wave circulator.

TX and RX while eliminating the need for high-quality millimeter-wave diplexers.

C. Millimeter-wave FD Relaying

Propagation loss is one of the main disadvantages of millimeter-wave wireless communication. Due to high propagation and absorption losses at high frequencies, the wireless link range is limited. To extend the link range as well as improve link margin, it would be useful to use relay nodes between sources and destinations [17]. However, traditional relay nodes are half-duplex (HD) and therefore have poor spectral efficiency or introduce unwanted latency in the network depending on whether FDD or TDD is used. Millimeter-wave FD relay nodes (depicted in Fig. 3) can be employed to extend the millimeter-wave link range, with significant spectral efficiency or latency improvement over existing HD relays. FD millimeter-wave relays can employ either separate antennas for TX and RX or a single antenna (Fig. 3). For the latter, a millimeter-wave circulator is required.

D. FMCW vehicular radar

One remaining problem in FMCW automotive radars is the TX-to-RX SI which is usually referred to as spillover. Spillover can result from on-chip coupling, limited isolation between the antennas or in the circulator, and from first reflections arising from the vehicle's fascia or from dirt or mud covering the antenna. The spillover power at the RX input can be much higher than the power reflected by targets that the radar aims to detect [18]. SI suppression techniques developed for millimeter-wave FD can also be adopted in automotive radars to solve the spillover problem. Additionally, another open problem in automotive radars is the design of fully-integrated low-loss circulators with high isolation to replace passive quasi-circulators (such as hybrids which have a theoretical loss of 3dB, typically 4dB) used at the shared-antenna interface.

E. Millimeter-wave FD wireless links for VR Headsets

Head-mounted displays create a virtual reality experience by projecting high quality video (e.g. 2160 x 1200 resolution) to each eye at a high frame rate (e.g. 90Hz) [19]. The video streams require very high data rate (approaching 20Gbps for emerging VR headsets) and need to be delivered with very low latency (less than 5ms) to prevent an adverse user experience

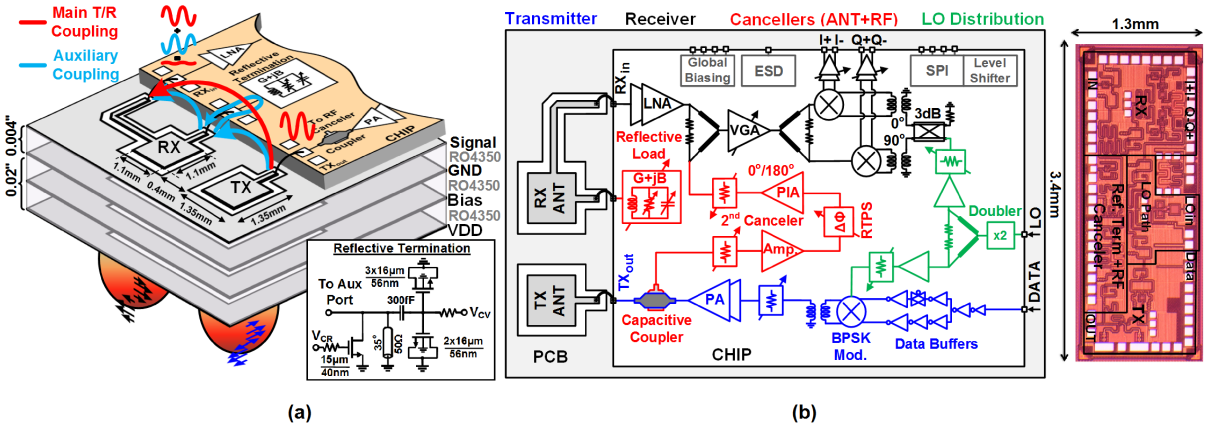

Fig. 4. (a) Polarization-based reconfigurable antenna cancellation concept and (b) the 60GHz SOI CMOS FD transceiver block diagram and chip photo.

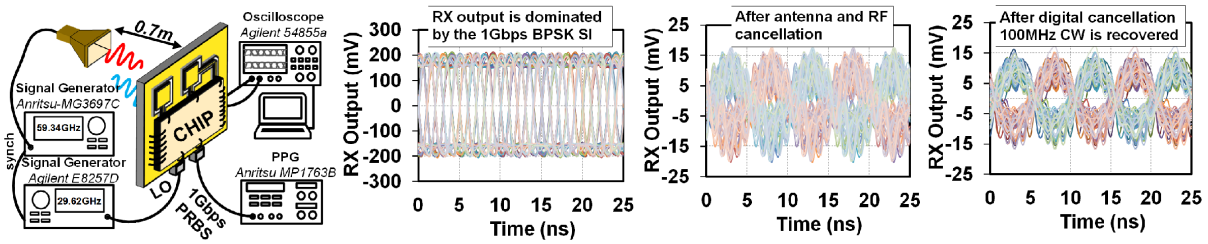

Fig. 5. 60GHz full-duplex link setup and demonstration.

(e.g. VR sickness) [20]. For a smooth VR experience, a huge amount of data has to be sent back and forth between the computer, the headset and the positional tracker, requiring bi-directional communication to close the feedback loop [19]. Millimeter-wave full-duplex wireless links have the potential of delivering high speed data with low latency and therefore can be a promising solution to cut the cord of VR headsets.

III. 60GHz 45nm SOI-CMOS Full-Duplex Transceiver

Recently, we reported the first FD transceiver which merges millimeter-wave with full-duplex [11], [12]. In our transceiver, a novel reconfigurable polarization-based antenna cancellation technique is proposed to enable millimeter-wave FD operation (Fig. 4(a)). As the RF signal is converted into an electromagnetic wave, polarization becomes another degree of freedom which can be leveraged. Our polarization-based antenna cancellation technique first employs a co-located transmit (TX) and receive (RX) antenna pair with orthogonal polarizations to reduce inherent TX-to-RX coupling, improving the initial isolation to 32-36dB over 54-66GHz based on simulations. Additionally, an indirect coupling path between TX and RX is created by introducing an auxiliary (AUX) port on the RX antenna that is co-polarized with the TX antenna. The AUX port is terminated with a high-order reconfigurable reflective termination that is integrated on the IC to achieve wideband self-interference (SI) cancellation at the RX port. The reflective termination reflects the coupled signal at the auxiliary port back into the antenna to the RX port to cancel the self interference at the RX input. An SI suppression of more than 50dB is achieved over 8 GHz bandwidth in simulation. The reflective termination is electronically programmable to maintain the high level of SI suppression even in the face of a changing EM environment.

Fig. 4(b) shows the architecture of our 45nm SOI CMOS 60GHz FD transceiver IC and its chip microphotograph [12]. It is a direct conversion BPSK transceiver consisting of five main parts: on-PCB T/R antenna pair with the polarization-based antenna cancellation, transmitter, receiver, a second RF canceller and LO distribution. The second RF cancellation path from the tranmitter output to the LNA output with >30dB gain control and >360° phase control (and a group delay of ≈93ps over 56-62GHz) is employed to further suppress the residual SI. In conjunction with digital cancellation in MATLAB, the FD transceiver achieves almost 80dB total SI suppression over 1GHz bandwidth. This allowed us to demonstrate the world's first millimeter-wave FD link over a distance of nearly 1m. Fig. 5 shows the link setup. As the desired signal, a continuous-wave signal at 100MHz offset from the LO frequency is transmitted from a horn antenna (with the same EIRP as our IC) while our 60GHz FD transceiver transmits a 1Gb/s BPSK signal. As can be seen, without any SI cancellation, the RX output is dominated by the 1Gb/s BPSK SI whereas after antenna, RF and digital cancellation, the desired CW signal is captured with a signal-to-interference-noise-and-distortion ratio of 7.2dB. It should be noted that the BPSK (SI) data rate and BW are the main indicators of the cancellation BW, not the desired CW signal. A BPSK signal with no pulse shaping

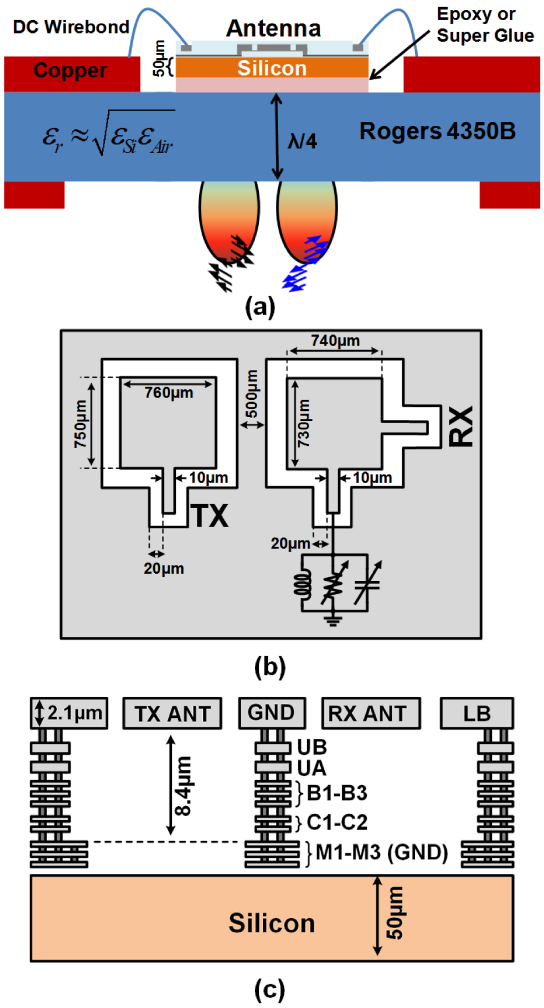

Fig. 6. On-chip implementation of the millimeter-wave slot loop T/R antenna pair with the proposed reconfigurable wideband polarization-based antenna cancellation technique: (a) cross-section of the proposed chip-PCB integration, (b) a 60GHz implementation in GF 45nm SOI CMOS, (c) GF 45nm SOI CMOS BEOL cross-section.

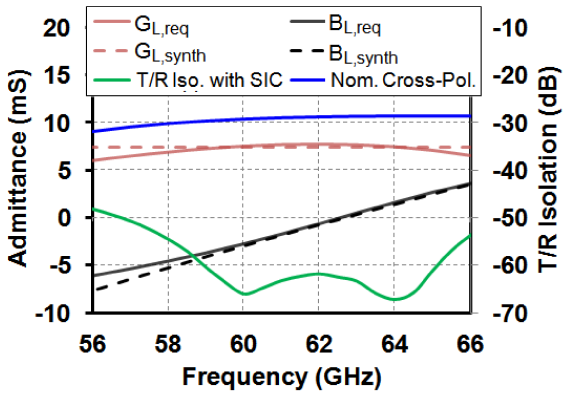

Fig. 7. 60GHz on-chip antenna cancellation simulations: required conductance and susceptance ($G_{L,req}$ and $B_{L,req}$), synthesized conductance and susceptance ($G_{L,synth}$ and $B_{L,synth}$), nominal isolation and isolation with SIC.

TABLE I
SUMMARY OF FULL-DUPLEX TRANSCEIVER PERFORMANCE

Implementation	**Technology**	45nm SOI CMOS
	Chip Area	1.3mm x 3.4mm
Transceiver Metrics	**Frequency**	57-66GHz
	Peak RX Conv. Gain	40dB (IEEE Channel-1) 32.7dB (IEEE Channel-2) 37.7dB (IEEE Channel-3) 38.2dB (IEEE Channel-4)
	RX Gain Control Range	~18dB (IEEE Channel-1) ~20dB (IEEE Channel-2) ~21dB (IEEE Channel-3) ~21dB (IEEE Channel-4)
	RX IP1dB (High Gain Mode)	-32dBm (IEEE Channel-1) -38dBm (IEEE Channel-2) -40dBm (IEEE Channel-3) -37dBm (IEEE Channel-4)
	RF NF	4dB
	TX Output Power	11-15dBm @ 56-66GHz
	Peak TX Efficiency	15.3% @ 57 GHz
	Data Rate	>5Gbps[1]
Full-Duplex Metrics	**SI Suppression**	>70dB (ANT+RF)
	SIC BW	1GHz @ 59GHz
	TX ANT Gain Degradation Due to SIC	1.1dB @ 60GHz (Simulated)
	RX ANT Gain Degradation Due to SIC	0.18dB @ 60GHz (Simulated)
	RX NF Degradation Due to SIC	Negligible (Measured)
	Full-Duplex Link	0.7m[2] (SINDR=7.2dBm)
Power Consumption	**TX+TX-side LO Dist**	206mW
	RX+RX-side LO Dist	111mW
	RF Canceller	44mW

[1] Loop-back test through the RF Canceller
[2] In conjunction with digital cancellation in MATLAB

has a sinc spectrum with a null-to-null BW that is twice the bit rate (or 2GHz in this case) and 90% of the energy is contained in 1.6× the bit rate (1.6GHz in this case). Since our transceiver is able to cancel a significant portion of the 1Gbps BPSK energy, we are able to see the desired CW signal. A similar cancellation performance is expected when the desired RX signal is also modulated at 1Gb/s. Table I summarizes the transceiver performance.

On-Chip Implementation of the Antenna Pair with Polarization-based Cancellation

Fig. 6 presents a method for the implementation of the SIC technique with on-chip slot loop antennas. The cross-section of the antenna-chip-PCB integration is shown in Fig. 6(a). The lossy Si substrate and CMOS back-end-of-line (BEOL) limitations pose challenges for the integration of high-gain, high-efficiency and wideband antennas. Since CMOS BEOL thickness (distance between top and bottom metal layers) is typically less than 10 μm, shielding the antenna from the lossy substrate results in current-based antennas radiating from the top with low efficiency [21], [22]. High-efficiency voltage-based antennas such as slot antennas with a quartz lens [23] or superstrate above the IC [24] can be implemented on chip but they suffer from bandwidth limitations. Therefore, we propose thinning the substrate down to 50 μm and taking the radiation from the bottom. The chip containing the antennas as well

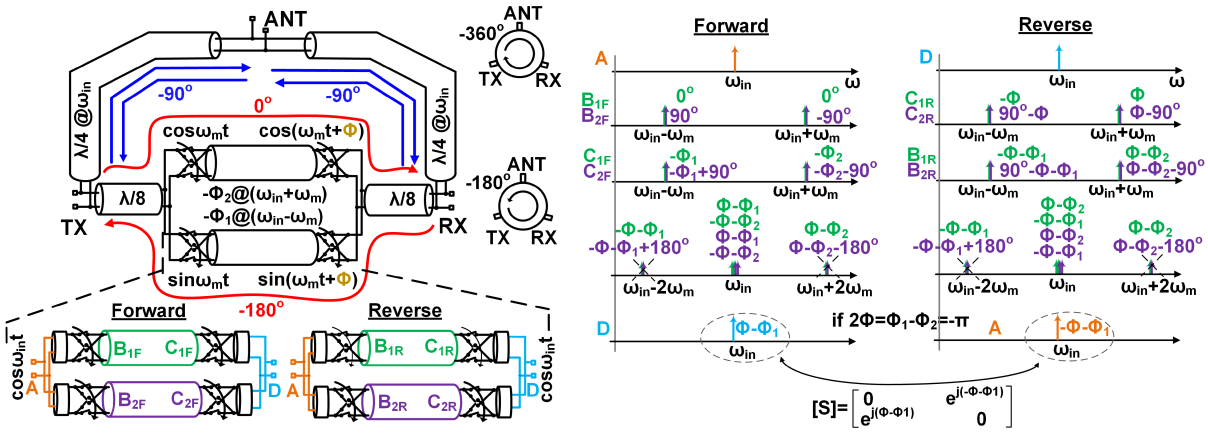

Fig. 8. Magnetic-free passive millimeter-wave circulator based on spatio-temporal conductance modulation.

as the FD millimeter-wave transceiver can be mounted on a PCB with $\epsilon_r = \sqrt{\epsilon_{air}\epsilon_{Si}}$ ≈3.45 (e.g. Rogers 4350B with ϵ_r=3.48 and tan(δ)=0.0037 at 10GHz) and $\lambda/4$ thickness using a non-conductive epoxy or superglue (ϵ_r ≈3.5 for both) which can be as thin as ≈50 μm. Thus, the wave impedance in Si is matched to the wave impedance in the air, improving the antenna efficiency (ratio of the total radiated power to the power delivered to the antenna).

Slot loop antennas have several advantages which make them favorable for on-chip integration. First, slot antennas help to meet the stringent CMOS metal density requirements, especially for the topmost metal, in the vicinity of the antennas. Additionally, slot loop antennas can be easily interfaced to the front-end circuits through coplanar waveguide (CPW) lines, which are the workhorses of millimeter-wave integrated circuit design as they easily satisfy metal density rules and provide good isolation between signal traces (typically higher than 50dB).

Fig. 6(b), Fig. 6(c) and Fig. 7 depict a 60GHz case study of the proposed on-chip T/R slot-loop antenna pair and SIC technique in the GF 45nm SOI CMOS process. The process offers 11 metal layers (Fig. 6(c)), including a 2.1 μm topmost aluminum layer (LB) in which the TX and RX antennas are implemented for high efficiency. The antennas are fed using conductor-backed CPW lines in LB with an M1-M3 bottom ground stack and M1-LB side grounds. The ground layer is removed under the antennas. The 60GHz T/R antenna core is simulated in IE3D with a 650 μm Rogers 4350B substrate layer assuming an epoxy thickness of 50 μm. The broadside TX and RX antenna gains are simulated as 0.15dB with 25% efficiency and -0.45dB with 22% efficiency, respectively. Fig. 7 shows the simulated required and synthesized conductance and susceptance in the reflective termination for perfect SIC across frequency. With an appropriately chosen parallel-RLC termination, a T/R isolation of more than 50dB is achieved over 10GHz bandwidth in simulation, completely covering the 60GHz IEEE 802.11ad band (57.24-65.88GHz).

IV. 28GHz Magnetic-free Non-reciprocal Passive 45nm SOI CMOS Circulator

Combining FD operation with beam-steering capability is essential to reveal the true benefits offered by millimeter-wave full-duplex. Therefore, millimeter-wave low-loss shared antenna interfaces with FD capability as well as high linearity, isolation and BW are extremely important in enabling small-form-factor shared TX-RX antenna arrays, especially for millimeter-wave 5G base stations that need to communicate with multiple users simultaneously.

Reciprocal, passive, matched 3-port shared-ANT interfaces, such as the electrical-balance duplexer (EBD) [25], have at least 3dB theoretical loss (typically 4dB at RF and millimeter-wave) in the TX-ANT and ANT-RX paths. This 3dB theoretical loss can be avoided by breaking Lorentz Reciprocity to realize non-reciprocal circulators. Traditionally, circulators have been implemented using ferrite materials that exhibit the Faraday effect under the influence of an external magnetic bias. In the recent years, there has been significant progress on breaking reciprocity with time-variance (and without the use of magnetic materials) [26], [27], specifically spatio-temporal permittivity modulation which is achieved using varactors in a circuit implementation. However, permittivity modulation has small modulation index (varactor C_{max}/C_{min} is typically 2-4) and therefore is not an effective solution for achieving non-reciprocity on silicon. Poor quality factor of varactors at millimeter-wave further limits the applicability of permittivity modulation at these frequencies. Inspired by the N-path filter-based low-RF CMOS circulator proposed in [28], [29], we recently proposed a near-28GHz fully integrated passive circulator in 45nm SOI CMOS based on the novel concept of spatio-temporal conductivity modulation. Our work marks the first demonstration of magnetic-free passive non-reciprocity at millimeter-wave. Spatio-temporal conductance modulation breaks phase non-reciprocity similar to the phase-shifted N-path filter of [28], [29], but requires modulation at a frequency lower than the operation frequency (1/3rd in this case), thus enabling millimeter-wave operation. It only requires four 50% duty-cycle I/Q phases as opposed to

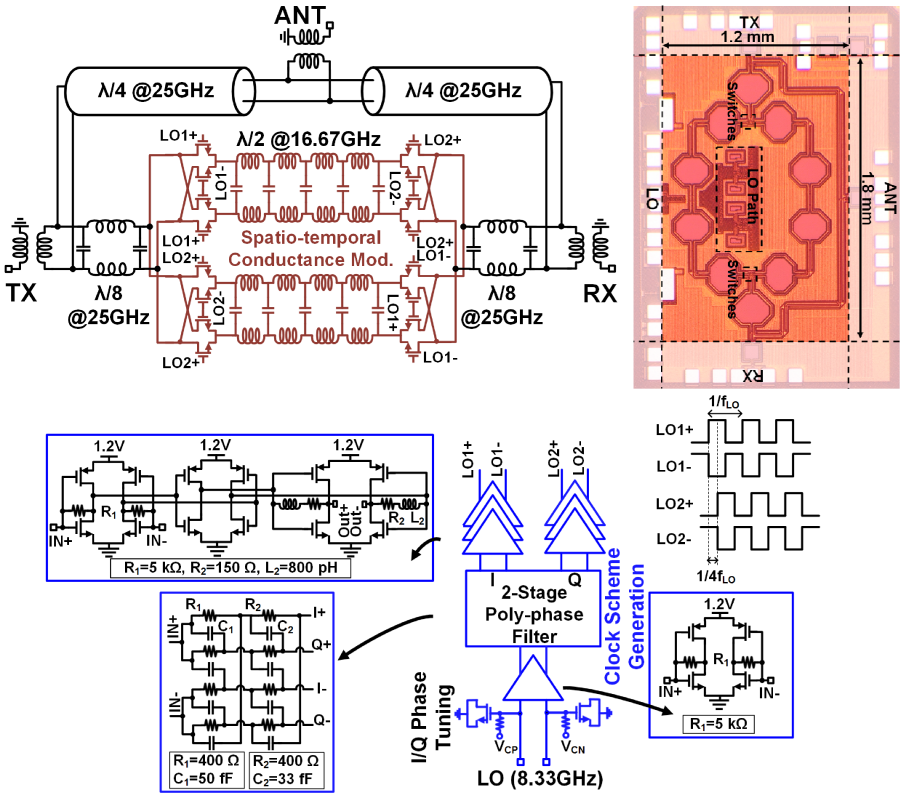

Fig. 9. Block and circuit diagram and chip photo of the near-28GHz 45nm SOI CMOS passive non-reciprocal circulator.

numerous low-duty-cycle non-overlapping clocks as in N-path filters, further easing millimeter-wave operation. Furthermore, the concept inherently enhances the insertion loss BW and isolation BW when compared with the N-path-filter-based approach of [28], [29]. This first demonstration of a passive non-reciprocal CMOS millimeter-wave circulator is scalable in frequency, e.g. to 60 or 77GHz, and, in principle, applicable from RF to optical frequencies.

Fig. 8 depicts the spatio-temporal conductance modulation operation based on a simple mixing analysis. It consists of two sets of I/Q switches on either end of I/Q transmission lines. The I/Q switches commutate the signal at a modulation frequency (ω_m) lower than the operating frequency (ω_{in}). As a result two mixing products appear after the commutation, at ω_{in}-ω_m and ω_{in}+ω_m. These signals flow through the transmission line which provides -Φ_1 and -Φ_2 phase shift at ω_{in}-ω_m and ω_{in}+ω_m, respectively. The phase shifted signals are then commutated again at ω_m but with a phase shift of Φ. If Φ=-90° and Φ_1-Φ_2=-180° (or equivalently, $2\omega_m T_d$=π, where T_d is the delay of the transmission line), a non-reciprocal phase shift with 180° difference between forward and reverse directions is achieved.

This non-reciprocal phase shift element can now be embedded within a 3λ/4 transmission line ring to realize a non-reciprocal circulator similar to [28], [29]. In Fig. 8, signal circulation is supported in only one direction (-270°-90° results in satisfaction of the boundary condition in the clockwise direction whereas -270°+90° results in violation of the boundary condition in the reverse direction). S-parameters of the non-reciprocal phase-shift element can be derived as S_{11}=S_{22}=0, S_{21}=$e^{-j\pi\omega_{in}/2\omega_m}$ and S_{12}=$e^{j\pi}e^{-j\pi\omega_{in}/2\omega_m}$, showing non-reciprocal phase-shift over an infinite bandwidth. The required phase shifts of S_{21}=$e^{+j\pi/2}$ and S_{12}=$e^{-j\pi/2}$ can be achieved at multiple frequencies, namely ω_{in}=$(4n-1)\omega_m$ where n is an positive integer, showing that the circulator operation frequency can be easily scaled up. For example, scaling the circulator to operate at 58.31GHz (ω_{in}=7ω_m) is as simple as designing the transmission line ring to be 3λ/4 at that frequency and keeping the non-reciprocal phase shift component unchanged.

Fig. 9 shows the implementation at 25GHz. The circulator is implemented in a differential fashion, reducing the LO feedthrough and improving power handling. The fully-balanced I/Q quads are designed using 2x16μm/40nm floating-body transistors. The non-reciprocal phase component is placed symmetrically between the TX and RX ports so that switch parasitics could be absorbed into the lumped capacitance of the λ/8 sections on either side. The λ/4 transmission lines between the TX and ANT and ANT and RX are implemented using differential conductor-backed co-planar waveguides. A two stage poly-phase filter (phase imbalance <2°) and self-biased differential inverter chains are used to generate the 8.33GHz square clocks.

Fig. 10 shows the measured small and large signal performance of the circulator. Small signal measurements were performed using on-chip probing with an Anritsu 37397E

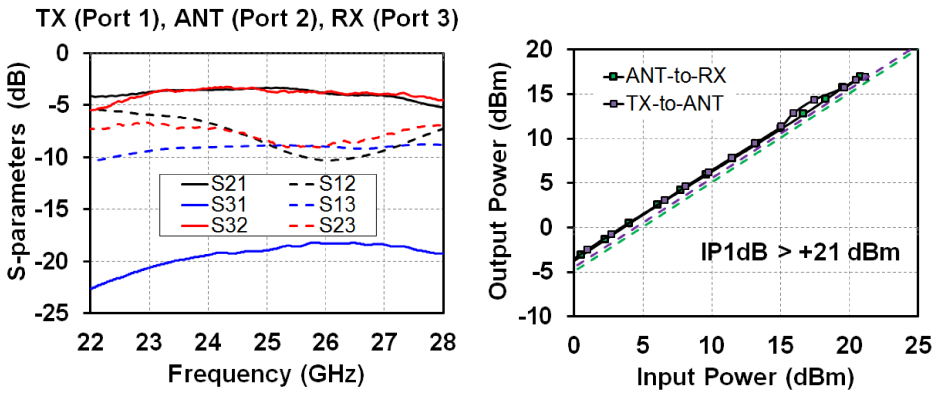

Fig. 10. Measured small and large signal performance of the near 28GHz fully-integrated non-reciprocal passive 45nm SOI CMOS circulator.

TABLE II
PERFORMANCE SUMMARY AND COMPARISON OF THE NEAR-28GHZ MAGNETIC-FREE CIRCULATOR TO THE STATE OF THE ART.

	TMTT'10[28]	TMTT'15 [27]	ISSCC'15 [22]	ISSCC'16 [26]	This work
Technique	Active Quasi Circulator	Active Quasi Circulator	Electrical Balance Duplexer	N-Path-Filter-based Magnetic-Free Passive Circulator	Magnetic-Free Passive Circulator Based on Spatio-Temporal Conductance Mod.
Technology	180nm CMOS	180nm CMOS	180nm SOI CMOS	65nm CMOS	**45nm SOI CMOS**
Frequency	24GHz	24GHz	1.9-2.2GHz	0.75GHz	**25GHz**
TX-ANT Transmission	+22.4dB	-5.7dB	-3.7dB	-1.7dB	**-3.3dB**
ANT-RX Transmission	+12.3dB	-5.7dB	-3.9dB	-1.7dB	**-3.2dB**
TX-RX Isolation	>15dB	>20 dB	>40dB	>20dB	**>18.5dB** [4]
Isolation BW [1]	~1%	~1.6%	~15%	4.3%	**18%** [5]
Center frequency/ Modulation frequency	N/A	N/A	N/A	1	**3**
Area	3.22mm^2	0.715mm^2	1.75mm^2	0.64mm^2/25mm^2 [2]	**2.16mm^2**
ANT-RX NF	17dB	N/R	3.9dB	4.3dB [3]	**3.3-4.4dB**
TX-ANT IP1dB	-19.8dBm	+9.5dBm	N/R	N/R	**>+21.5dBm**
TX-ANT IIP3	-11dBm	N/R	+70dBm	+27.5dBm	**+19.9dBm**
P_{DC}	144.8mW	7.2mW	0	59mW	**78.4mW**

[1] BW over which an isolation better than the value quoted in the row above is maintained.
[2] Includes SMD inductors on PCB.
[3] Includes 2dB degradation due to LO phase noise.
[4] Limited by the mmWave test setup.
[5] This is the 1dB insertion loss BW.
N/A: Not Applicable, N/R: Not Reported

65GHz 2-port VNA while a millimeter-wave probe terminated with an Anritsu V210 50Ω termination was landed on the third port. The 25GHz circulator achieves 3.3dB/3.2dB TX-to-ANT/ANT-to-RX insertion losses (IL), respectively, and 18.3-21.2dB of TX-to-RX ISO over the 4.6GHz 1dB IL BW. This near-20dB isolation is limited by reflections at the antenna port due to imperfect matching, a challenge for all circulators. At millimeter-wave, it is hard to obtain better than -20dB reflection coefficient from a millimeter-wave probe and termination combination. Integrated antenna tuners or balance networks are required to mitigate this limitation.The measured ANT-to-RX NF and TX-to-ANT/ANT-to-RX input P1dB are 3.3-4.2dB and >21dBm (Fig. 10), respectively. The P1dBs are high relative to the IIP3s (+19.9dBm) because the circulator gracefully transitions to reciprocal operation under large-signal operation. Since IIP3 is just an extrapolation from measurements with small input signals, this transition cannot be captured and thus the traditional estimation between P1dB and IIP3 values does not hold.

Table II compares this circulator with prior art. It performs better than active millimeter-wave circulators [30], [31] in all metrics (loss, linearity, NF and BW). When compared with a passive EBD [25], this work achieves >1dB overall advantage in IL (the sum of TX-to-ANT and ANT-to-RX ILs) while operating at >10x higher frequency. When compared with the N-path filter-based circulator of [28], [29], this work significantly enhances BW and most importantly scales to millimeter-wave.

V. Conclusion

Millimeter-wave FD can offer wide bandwidths with increased spectral efficiency and can be used in many applications ranging from small-cell 5G base-stations, backhaul and FMCW radar to wireless links for virtual reality. However, the SI from the transmitter to its own receiver poses a tremendous challenge and novel millimeter-wave SI suppression techniques are required. This paper reviewed recent research efforts on millimeter-wave FD and SI suppression techniques at Columbia University, specifically the first 60GHz FD CMOS transceiver and 25GHz fully-integrated magnetic-free non-reciprocal passive circulator. Topics for future research include techniques to improve the power handling of integrated non-reciprocal circulators, novel integrated antenna tuners for millimeter-wave non-reciprocal circulators, and demonstration of millimeter-wave full-duplex operation within phased arrays. Device stacking techniques that have been investigated in SOI processes for T/R switches as well as PAs can be explored to improve the power handling capability of on-chip circulators. Bootstrapping is another technique that can be used to improve the linearity and power handling of switch-based circulators.

Acknowledgment

This work was supported by Global Foundries, DARPA grants FA8650-14-1-7414 and FA8650-16-1-7644, and NSF grant EFMA 1641100.

References

[1] A. Natarajan, S. K. Reynolds, M. D. Tsai, S. T. Nicolson, J. H. C. Zhan, D. G. Kam, D. Liu, Y. L. O. Huang, A. Valdes-Garcia, and B. A. Floyd, "A fully-integrated 16-element phased-array receiver in SiGe BiCMOS for 60-GHz communications," *IEEE Journal of Solid-State Circuits*, vol. 46, no. 5, pp. 1059–1075, May 2011.

[2] Y. A. Li, M. H. Hung, S. J. Huang, and J. Lee, "A fully integrated 77GHz FMCW radar system in 65nm CMOS," in *2010 IEEE International Solid-State Circuits Conference*, Feb 2010, pp. 216–217.

[3] J. Hasch, E. Topak, R. Schnabel, T. Zwick, R. Weigel, and C. Waldschmidt, "Millimeter-wave technology for automotive radar sensors in the 77 GHz frequency band," *IEEE Transactions on Microwave Theory and Techniques*, vol. 60, no. 3, pp. 845–860, March 2012.

[4] J. Zander and P. Mahonen, "Riding the data tsunami in the cloud: myths and challenges in future wireless access," *IEEE Communications Magazine*, vol. 51, no. 3, pp. 145–151, March 2013.

[5] J. G. Andrews, S. Buzzi, W. Choi, S. V. Hanly, A. Lozano, A. C. K. Soong, and J. C. Zhang, "What will 5G be?" *IEEE Journal on Selected Areas in Communications*, vol. 32, no. 6, pp. 1065–1082, June 2014.

[6] Y. Zhu, Z. Zhang, Z. Marzi, C. Nelson, U. Madhow, B. Y. Zhao, and H. Zheng, "Demystifying 60GHz outdoor picocells," in *Proceedings of the 20th Annual International Conference on Mobile Computing and Networking*. New York, NY, USA: ACM, 2014, pp. 5–16.

[7] P. M. N. H. Mahmood, G. Berardinelli and F. Frederiksen, "Throughput analysis of full duplex communication with asymmetric traffic in small cell systems," in *International Conference on Wireless and Mobile Communications*, Oct. 2015.

[8] J. Marasevic and G. Zussman, "On the capacity regions of single-channel and multi-channel full-duplex links," in *Proc. ACM MobiHoc'16*, Jul. 2016.

[9] A. Sabharwal, P. Schniter, D. Guo, D. Bliss, S. Rangarajan, and R. Wichman, "In-band full-duplex wireless: Challenges and opportunities," *IEEE Journal on Selected Areas in Communications*, vol. 32, no. 9, pp. 1637–1652, Sept 2014.

[10] J. Zhou, T.-H. Chuang, T. Dinc, and H. Krishnaswamy, "Integrated wideband self-interference cancellation in the RF domain for FDD and full-duplex wireless," *IEEE J. Solid-State Circuits*, vol. PP, no. 99, pp. 1–17, 2015.

[11] T. Dinc, C. A., and H. Krishnaswamy, "A 60GHz same-channel full-duplex CMOS transceiver and link based on reconfigurable polarization-based antenna cancellation," in *IEEE Proc. RFIC'15*, 2015.

[12] T. Dinc, A. Chakrabarti, and H. Krishnaswamy, "A 60 GHz CMOS full-duplex transceiver and link with polarization-based antenna and rf cancellation," *IEEE Journal of Solid-State Circuits*, vol. 51, no. 5, pp. 1125–1140, May 2016.

[13] T. Dinc and H. Krishnaswamy, "A 28GHz magnetic-free non-reciprocal passive CMOS circulator based on spatio-temporal conductance modulation," in *to appear in 2017 IEEE International Solid-State Circuits Conference (ISSCC)*, Feb 2017.

[14] R. Taori and A. Sridharan, "Point-to-multipoint in-band mmwave backhaul for 5G networks," *IEEE Communications Magazine*, vol. 53, no. 1, pp. 195–201, January 2015.

[15] "Crucial economics for mobile data backhaul:An analysis of the total cost of ownership of point-to-point, point-to-multipoint, and fiber options," in *by Senza Fili Consulting*, 2012.

[16] "EdgeHaul millimeter wave small cell backhaul system," Mar. 2015. [Online]. Available: http://www.interdigital.com/presentations/edgehaul-millimeter-wave-small-cell-backhaul-system

[17] Z. Wei, X. Zhu, S. Sun, Y. Huang, A. Al-Tahmeesschi, and Y. Jiang, "Energy-efficiency of millimeter-wave full-duplex relaying systems: Challenges and solutions," *IEEE Access*, vol. 4, pp. 4848–4860, 2016.

[18] D. Guermandi, Q. Shi, A. Medra, T. Murata, W. V. Thillo, A. Bourdoux, P. Wambacq, and V. Giannini, "A 79GHz binary phase-modulated continuous-wave radar transceiver with TX-to-RX spillover cancellation in 28nm CMOS," in *2015 IEEE International Solid-State Circuits Conference - (ISSCC) Digest of Technical Papers*, Feb 2015, pp. 1–3.

[19] "How Oculus Rift works: Everything you need to know about the VR sensation," Mar. 2016. [Online]. Available: https://www.wareable.com/oculus-rift/how-oculus-rift-works

[20] "IEEE 802.11TGay use cases," Sep. 2015. [Online]. Available: https://mentor.ieee.org/802.11/dcn/15/11-15-0625-03-00ay-ieee-802-11-tgay-usage-scenarios.pptx

[21] Y. Zhang, M. Sun, and L. Guo, "On-chip antennas for 60-GHz radios in silicon technology," *IEEE Transactions on Electron Devices*, vol. 52, no. 7, pp. 1664–1668, July 2005.

[22] T. Yao, L. Tchoketch-Kebir, O. Yuryevich, M. Gordon, and S. Voinigescu, "65GHz doppler sensor with on-chip antenna in 0.18μm SiGe BiCMOS," in *IEEE Proc. of International Microwave Symp.*, June 2006, pp. 1493–1496.

[23] J. Edwards and G. Rebeiz, "High-efficiency silicon RFIC millimeter-wave elliptical slot-antenna with a quartz lens," in *IEEE International Symposium on Antennas and Propagation*, July 2011, pp. 899–902.

[24] J. Edwards, G. Rebeiz, D. Titz, F. Ferrero, and C. Luxey, "High-efficiency elliptical-slot silicon RFIC antenna with quartz superstrate," in *Antennas and Propagation Society International Symposium (APSURSI)*, July 2012, pp. 1–2.

[25] B. van Liempd, B. Hershberg, K. Raczkowski, S. Ariumi, U. Karthaus, K. F. Bink, and J. Craninckx, "2.2 a +70dBm IIP3 single-ended electrical-balance duplexer in 0.18um SOI CMOS," in *2015 IEEE International Solid-State Circuits Conference*, Feb 2015, pp. 1–3.

[26] S. Qin, Q. Xu, and Y. E. Wang, "Nonreciprocal components with distributedly modulated capacitors," *IEEE Transactions on Microwave Theory and Techniques*, vol. 62, no. 10, pp. 2260–2272, Oct 2014.

[27] N. A. Estep, D. L. Sounas, and A. Al, "Magnetless microwave circulators based on spatiotemporally modulated rings of coupled resonators," *IEEE Transactions on Microwave Theory and Techniques*, vol. 64, no. 2, pp. 502–518, Feb 2016.

[28] N. Reiskarimian and H. Krishnaswamy, "Magnetic-free non-reciprocity based on staggered commutation," *Nature Communications*, vol. 7, no. 11217, April 2016.

[29] J. Zhou, N. Reiskarimian, and H. Krishnaswamy, "Receiver with integrated magnetic-free N-path-filter-based non-reciprocal circulator and baseband self-interference cancellation for full-duplex wireless," in *2016 IEEE International Solid-State Circuits Conference (ISSCC)*, Jan 2016, pp. 178–180.

[30] J.-F. Chang, J.-C. Kao, Y.-H. Lin, and H. Wang, "Design and analysis of 24-GHz active isolator and quasi-circulator," *IEEE Transactions on Microwave Theory and Techniques*, vol. PP, no. 99, pp. 1–12, 2015.

[31] H. S. Wu, C. W. Wang, and C. K. C. Tzuang, "CMOS active quasi-circulator with dual transmission gains incorporating feedforward technique at K-Band," *IEEE Transactions on Microwave Theory and Techniques*, vol. 58, no. 8, pp. 2084–2091, Aug 2010.